差强差厚三层板电阻点焊熔核尺寸的控制方法

沈 洁， 林浩磊， 张延松， 陈关龙
(上海交通大学 上海市数字化汽车车身工程重点实验室，上海 200240)

沈 洁

摘 要：针对差强差厚三层板电阻点焊过程熔核形成规律展开研究，提出采用不对称电极帽匹配方法改善点焊熔核尺寸及可焊性窗口宽度. 基于建立的有限元模型，分析了两种电极帽匹配下薄板侧熔核形成过程中的电流密度、温度场及熔核尺寸的变化规律. 通过试验对比分析了不同焊接时刻的薄板侧熔核尺寸，并建立了两种电极帽匹配下的差强差厚三层板点焊可焊性工艺窗口. 结果表明，该方法能有效解决差强差厚三层板点焊过程中的熔核偏移及薄板侧熔核尺寸偏小的问题，提高电阻点焊过程的鲁棒性.

关键词：三层板；电阻点焊；熔核尺寸；可焊性工艺窗口
中图分类号：TG 115.21 **文献标识码**：A **文章编号**：0253－360X(2012)01－0033－04

0 序 言

应对汽车节能减排与车身轻量化的技术需求，以双相钢为代表的先进高强钢材料在车身中的应用越来越多，在车身前纵梁、A，B，C柱等很多部位会出现强度、厚度都不同的三层板电阻点焊应用情况，且应用的比例正在逐年增加. 例如：上海某汽车公司在新车型开发中，差强差厚三层板电阻点焊应用比例达到33%. 因此，差强差厚三层板的电阻点焊质量已成为车身制造中值得关注的问题之一[1-5].

受材料属性、板材厚度的影响，差强差厚三层板电阻点焊通电过程中，上下板材与中间板材接触面电流密度分布不均，随着通电时间增加，上下接触面间生热不一致，焊点熔核向厚板侧发生偏移，薄板侧熔核尺寸将小于厚板侧熔核尺寸[6]. 当焊接参数较小时，薄板侧熔核尺寸难以满足质量要求，易出现虚焊问题. 焊接参数较大时，又会发生强飞溅问题，造成差强差厚三层板的点焊可焊性工艺窗口狭窄. 为保证三层板焊点质量，控制三层板两侧熔核形成规律是提高薄板侧熔核尺寸的有效手段.

传统点焊质量控制方法通过单一改变焊接电流、时间和电极压力等焊接参数难以协调两侧熔核的生成与长大. 为此，文中提出采用不对称电极帽端面直径匹配的方法来改善差强差厚三层板点焊过程中两侧熔核的形成规律. 首先通过有限元方法对比分析了薄板侧熔核形成过程中的电流密度、温度的变化规律及最终的熔核尺寸. 其次，通过试验比较了不同焊接时间下薄板侧熔核的尺寸，最后对比分析了两种电极帽匹配下的点焊可焊性窗口变化.

收稿日期：2010－10－22
基金项目：国家自然科学基金资助项目(50905111)；上海汽车工业科技发展基金资助项目(0907)

1 熔核形成过程的有限元仿真

1.1 三层板点焊模型

文中以顺序由上至下依次0.7 mm DC04，1.4 mm DP600和1.8 mm DP780的三层板匹配为例，采用两种电极帽匹配(图1，采用对称电极帽匹配时，端面直径 $E_1=E_2=5$ mm，以下简称“5+5匹配”；采用不对称电极帽匹配时，$E_1=4$ mm，$E_2=6$ mm，以下简称“4+6匹配”)，其中尺寸 E_1，E_2 分别为上、下电极帽端面直径，尺寸 D_1 为薄板侧的熔核直径，点 P_1 为薄板侧结合面中心点.

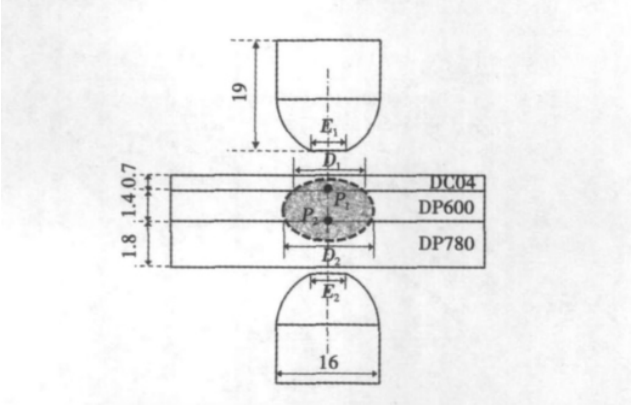

图1 板材匹配顺序及电极帽尺寸(mm)
Fig. 1 Dimensions of specimen and electrode caps

利用 ANSYS 软件建立三层板电阻点焊有限元模型. 电流均匀地从电极顶部施加给上电极,热量通过对流传向周围空气,对流传热系数为 19.4 W/(m²·K);钢板远端的温度、铜电极内部水的温度均假设为周围温度;分析点焊过程中的变形时,热载荷(即温度)施加在每个节点上,同时允许对称轴沿垂直方向延伸而不允许有横向位移,相关材料、工艺参数选择见文献[5].

1.2 仿真结果分析

点焊过程通电 20 ms 后,两种不同端面直径电极帽匹配下的电流密度分布如图 2 所示. 其中,图 2a 为 5+5 匹配下的电流密度矢量图,图 2b 为 4+6 电极帽匹配下的电流密度矢量图. 可以看出:4+6 匹配下薄板与中间板结合面上的电流密度明显高于 5+5 匹配下薄板与中间板结合面上的电流密度.

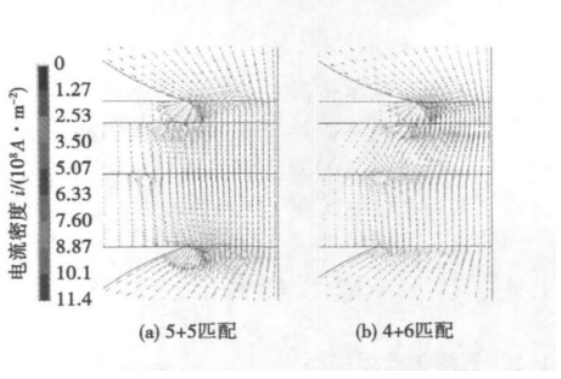

图 2 不同电极帽匹配下电场图(通电时间 20 ms)

Fig. 2 Comparison of current density using FEM

两种电极帽匹配下薄板侧结合面中心温度随时间的变化情况如图 3 所示. 电极压力 4.3 kN,电流 8.5 kA,通电时间 120×3 ms. 在前 120 ms 内,4+6 匹配下薄板侧结合面中心温度上升速率明显快于 5+5 匹配下薄板侧结合面中心温度上升速率. 在后 240 ms 内,温度上升减缓,通电过程结束后,4+6 匹配下温度更高. 通电过程结束后的熔核尺寸如图 4 所示. 采用 5+5 电极帽匹配,薄板侧熔核尺寸为 4.58 mm,而采用 4+6 电极帽匹配后,薄板侧熔核增大至 5.84 mm. 可见不对称电极帽端面直径改变了薄板侧温度场分布,更利于薄板侧熔核的形成,薄板侧熔核尺寸增大明显.

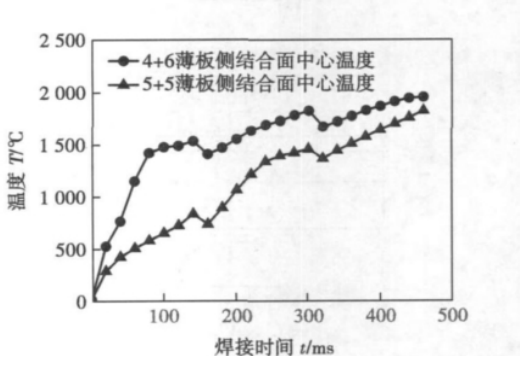

图 3 不同电极帽匹配下薄板侧熔核中心温度变化曲线

Fig. 3 Comparison of temperature histories of P1

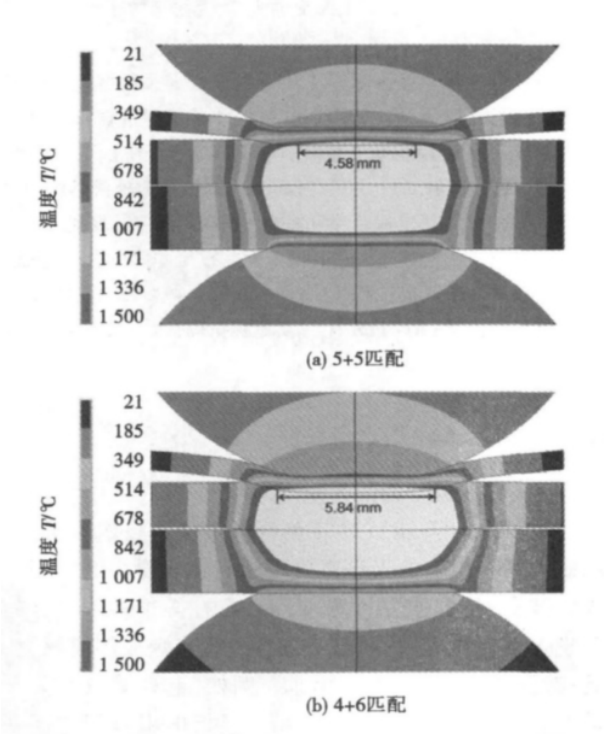

图 4 不同电极帽匹配下薄板侧熔核尺寸(通电时间 360 ms)

Fig. 4 Comparison of nugget size using FEM

2 熔核形成过程的试验分析

2.1 试验条件

试验所用机器人为 FANUC R-2000iA 型六轴机器人,重复定位精度为 ±5 μm. 焊枪为日本 OBARA 公司的 DC 型伺服焊枪[7]. 三种板材的化学成分如表 1 所示. 由于数值分析时采用 8.5 kA 电流值不能得到合格焊点(合格直径标准为 $5t^{1/2}$[8],t 为中间板厚,t = 1.4 mm,$5t^{1/2}$ 约为 6 mm),进一步增大焊接电流时,数值分析结果发现:当焊接电流增大至 9.1 kA 时,4+6 电极帽匹配下熔核尺寸能达到 6 mm,而 5+5 电极帽匹配下仍未达到 6 mm 的标准,为更好地研究两种电极帽匹配对熔核形成规律及可焊性窗口的影响,试验时焊接电流取 9.1 kA,通电阶段包含三段脉冲,每段脉冲时间为 120 ms,相邻脉冲之间的冷却时间为 20 ms,试验电极压力为 4.3 kN.

2.2 熔核尺寸的试验结果与讨论

为验证数值分析获得的两种电极帽匹配下三层

表 1　三种钢板的化学成分(质量分数,%)

Table 1　Chemical compositions of three steels

材料	C	Mn	P	S	Al	Si
DC04	<0.08	<0.40	<0.025	<0.020	>0.020	—
DP600	<0.18	<2.20	<0.035	<0.030	>0.020	<0.80
DP780	<0.20	<2.50	<0.035	<0.030	>0.020	<0.80

板电阻点焊薄板侧熔核的形成规律,分别从焊接时间 360 ms 开始,每减小 40 ms 焊接一个试样,对试样薄板侧进行剥离,直至没有熔核生成为止. 两种电极帽匹配下薄板侧熔核尺寸随通电时间的变化如图 5 所示.

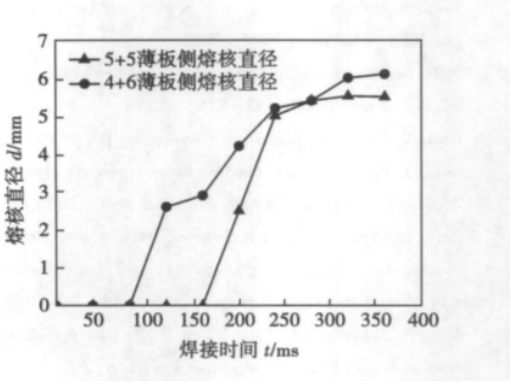

图 5　不同电极帽匹配下薄板侧熔核尺寸曲线(剥离试验)

Fig. 5　Comparison of nugget sizes by peel test

试验结果表明: 采用 5 + 5 电极帽匹配时,薄板侧在通电 200 ms 后开始形成熔核. 焊接结束时,薄板侧熔核尺寸为 5.7 mm. 采用 4 + 6 电极帽匹配时,薄板侧熔核在通电 120 ms 时就开始形成,比 5 + 5 匹配下薄板侧熔核开始形成优先 80 ms. 焊接结束时,薄板侧的最终熔核尺寸为 6.2 mm,比 5 + 5 匹配下薄板侧最终熔核尺寸大 0.5 mm. 由此可以看出,上、下电极分别采用 4 mm 和 6 mm 端面直径电极帽,可以改变熔核形成规律,使薄板侧熔核优先形成并最终得到更好的熔核尺寸,这与数值分析结果一致.

为更好地观察两种电极帽匹配对薄板侧熔核形成规律的影响,分别在每个通电脉冲结束后对试样进行金相试验,如图 6 所示. 试验发现,在 120 ms 时,5 + 5 匹配下薄板侧结合面有明显的界限,未形成熔核,4 + 6 匹配下薄板侧熔核尺寸为 2.66 mm(图 6 a),这是由于采用不对称电极帽可以提高薄板侧结合面电流密度,使得熔核优先形成; 随着时间的增长,热量不断积累,温度不断升高,在 240 ms 时,5 + 5 匹配下薄板侧熔核尺寸为 4.72 mm,4 + 6 匹配下薄板侧熔核尺寸达到 5.21 mm(图 6 b); 通电过程结束后,5 + 5 匹配下薄板侧熔核尺寸为 5.56 mm,4 + 6 匹配下薄板侧熔核尺寸为 6.11 mm(图 6 c). 可见,采用不对称电极帽匹配能有效提高薄板侧熔核尺寸.

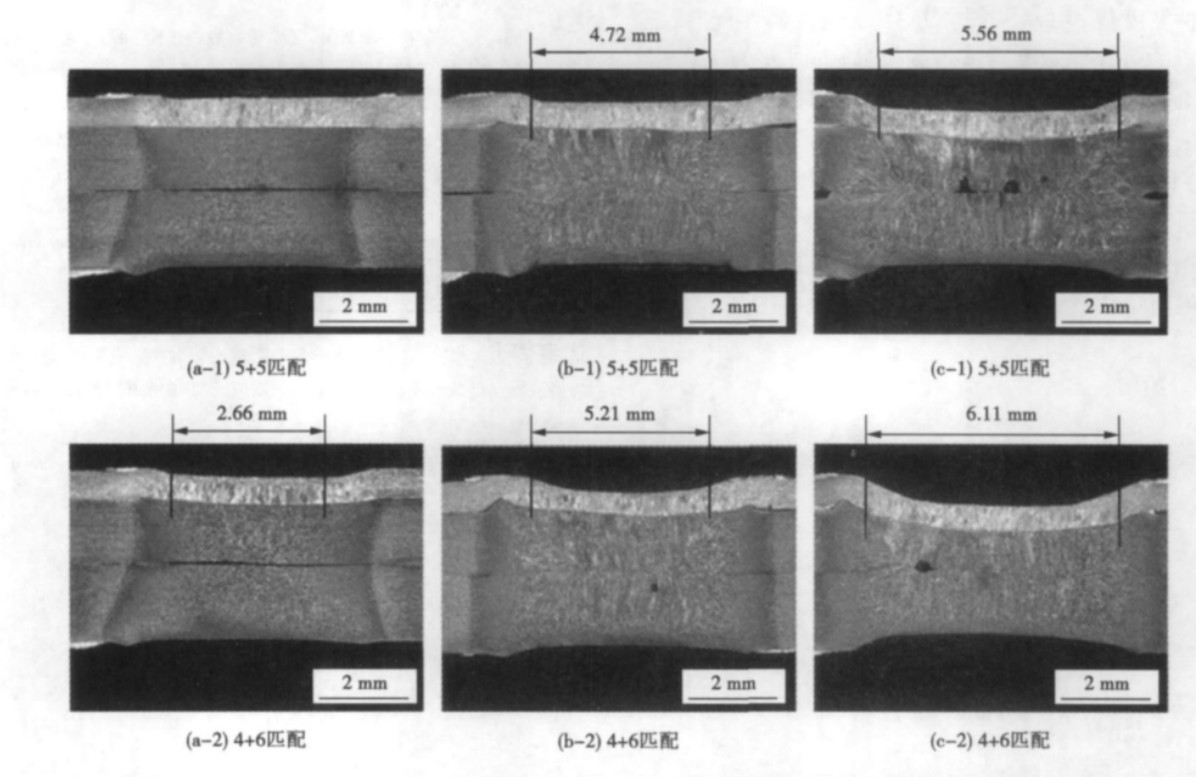

图 6　不同通电时间下三层板薄板侧熔核尺寸图(金相试验)

Fig. 6　Comparison of nugget sizes by metallurgical examination

2.3 可焊性窗口试验结果与讨论

为分析两种电极帽匹配对可焊性工艺窗口宽度的影响，分别制定两种电极帽匹配下的可焊性窗口. 试验开始时电极预磨100点，使得电极帽端面状态稳定. 选取不同的焊接时间，逐次增大焊接电流，幅度为100 A/次，以薄板侧焊点熔核直径达到合格时的电流值为左边界；继续增大焊接电流，幅度为200 A/次，以焊点刚开始发生飞溅时的电流值为右边界. 两种电极帽匹配下的可焊性窗口如图7所示.

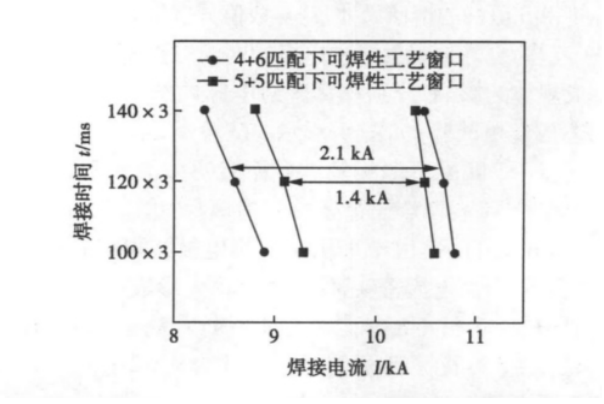

图7 不同端面直径电极帽匹配下的点焊工艺窗口

Fig. 7 Comparison of weld lobes

由图7以看出，采用5+5电极帽匹配时，三层板可焊性宽度较窄，在通电时间为120×3 ms时，可焊性宽度仅为1.4 kA；采用4+6电极帽匹配时，三层板的可焊性宽度明显变宽，在通电时间为120×3 ms时，可焊性宽度达到2.1 kA. 同时，与上下电极均采用5 mm端面直径电极帽的可焊性窗口相比，上、下电极分别采用4 mm和6 mm端面直径电极帽的可焊性窗口中的左边界偏左约500 A，这意味着，采用4 mm + 6 mm匹配的电极帽可以在较小的焊接电流下生成合格的焊点.

3 结 论

(1) 文中提出采用不对称电极端面尺寸方法，解决了差强差厚三层板点焊过程中的熔核偏移及薄板侧熔核尺寸偏小的问题.

(2) 以0.7 mm DC04 + 1.4 mm DP600 + 1.8 mm DP780的三层板匹配为例，当采用4+6电极帽匹配时，薄板侧熔核形成时刻提前并最终得到更大的熔核尺寸，可焊性工艺窗口宽度由1.4 kA拓宽至2.1 kA，符合生产实际要求.

参考文献：

[1] Ma N, Murakawa H. Numerical and experimental study on nugget formation in resistance spot welding for three pieces of high strength steel sheets [J]. Journal of Materials Processing Technology, 2010, 210(14): 2045 - 2052.

[2] Schreiber S. Investigations into three-member welding [J]. Welding and Cutting, 2001, 53: E252 - E259.

[3] Coon T, Elliott A, Joaquin A. Resistance spot weldability of three metal stack dual phase 600 hot-dipped galvanized steel [C] // 2007 world congress, Detroit, Michigan April, 2007: 16 - 19.

[4] Sin S R, Yang S M, Yu H S, *et al*. Fatigue analysis of multi-lap spot welding of high strength steel by quasi static tensile-shear test [J]. Key Engineering Materials, 2007, 345 - 346: 251 - 254.

[5] Kang H T, Accorsi I, Patel B, *et al*. Fatigue performance of resistance spot welds in three sheet stack-ups [J]. Procedia Engineering, 2010, 2(1): 129 - 138.

[6] Shen J, Zhang Y S, Lai X M. Modeling of resistance spot welding of multiple stacks of steel sheets [J]. Materials and Design, 2001, 32(2): 550 - 560.

[7] 孙海涛，张延松，来新民，等. 变电极力作用下的电阻点焊质量分析 [J]. 焊接学报，2008，29(6)：45 - 48.
Sun Haitao, Zhang Yansong, Lai Xinmin, *et al*. Quality of resistance spot welding based on variable electrode force [J]. Transactions of the China Welding Institution. 2008, 29(6): 45 - 48.

[8] ANSI/AWS/SAE/D8.9-97. Recommended practices for test methods for evaluating the resistance spot welding behavior of automotive sheet steel materials [S]. American Welding Society, 1997.

作者简介： 沈 洁，男，1983年出生，博士研究生. 主要研究方向为多层板点焊数值模拟及质量控制. 发表论文10余篇. Email: shen_jie@sjtu.edu.cn

通讯作者： 张延松，男，副教授. Email: zhangyansong@sjtu.edu.cn

pp 17 – 20

Abstract: Diffusion bonding of TiAl to Ni-based alloy using Ti interlayer was studied. The microstructure of the joint and effect of bonding temperature on microstructure and properties of the joint were investigated, and the mechanism of the formation of reaction layers was also discussed. The experiment results show that the interfacial structure of the GH99/Ti/TiAl joint is GH99/(Ni,Cr)$_{ss}$/rich Ti-(Ni,Cr)$_{ss}$/TiNi/Ti_2Ni/α-Ti + Ti_2Ni/Ti(Al)$_{ss}$/TiAl + Ti_3Al/TiAl. With the bonding temperature increasing, the thickness of reaction layers increases. The shear strength of the joint increases with the bonding temperature, and goes through a maximum at 1173 K/30 min/20 MPa and thereafter falls off. The maximum shear strength is 260.7 MPa.

Key words: titanium aluminium alloy; Ni-based superalloy; diffusion bonding; interfacial structure

Microstructure and properties of radial friction welded joint of 37CrMnMo steel pipe QIN Guoliang[1], ZHANG Chunbo[2], ZHOU Jun[2], QI Xiubin[2], ZHANG Yan[2] (1. Institute of Advanced Welding Technology, Shandong University, Jinan 250061, China; 2. Harbin Welding Institute, Harbin 150080, China). pp 21 – 24

Abstract: With self-developed radial friction welding machine, 37CrMnMo steel pipe was welded at the optimized welding parameters by taking 45 steel as ring. Experimental results show that the ring has serious plastic deformation and there is a narrow HAZ in 37CrMnMo steel pipe body and the weld is oxidized. The mean shear strength of the weld can be up to 401 MPa, which is higher than that of 45 steel. The appearance of shear fracture is smooth and characterized by shear dimple, which indicates that the weld has high ductile and plastic properties. The microhardness is decreased from the bonding center to both sided of 45 steel ring and 37CrMnMo steel pipe. The analyses on microstructure of the joint show that there is a very good narrow metallurgical bonding zone between steel ring and steel pipe, but overheated zones appears in HAZ of 45 steel pipe and 20 steel ring. The HAZ in 45 steel side is ferrite, pearlite and bainite, and that in 37CrMnMo steel side is bainite and a few martensite. Compared with base metal, hardening microstructure appears in HAZs of 45 steel and 37CrMnMo steel because of high cooling rate, but the microstructure in the weld is finer than that of base metal under the thermo-mechanical coupling interaction.

Key words: radial friction welding; steel pipe welding; joint; microstructure; mechanical properties

Welding currents filtering of compulsively short circuiting transfer in rotational arc MAG welding GAO Yanfeng[1,2], XIAO Jianhua[1], ZHANG Hua[2] (1. School of Aeronautical Manufacturing Engineering, Nanchang Hangkong University, Nanchang 330063, China; 2. School of Mechanical & Electrical Engineering, Nanchang University, Nanchang 330031, China). pp 25 – 28

Abstract: The present paper describes the welding current characteristics of rotational arc MAG welding in V groove. It is found that the compulsively short circuiting transfer would take place when the welding gun rotates to the sides of V groove. The reason for this phenomenon is that the contact tip distance between the wire tip and workpiece becomes short when the welding gun moves to the sides of groove. During the period of short circuiting transfer, the welding currents would sharply increase, so as to affect the rotational arc sensor sensitivity. A hybrid filtering method based on spatial neighborhood mean filter and soft threshold wavelet filter is proposed to process the welding currents, and the real-time characteristics of this method is researched in this paper as well. The experimental results show that the hybrid filtering method has a higher filtering property and better real-time character. This study will set up the foundation for the welding gun deviation identification in the welding seam tracking.

Key words: rotational arc welding; short circuiting transfer; welding currents; wavelet filtering

Laser-arc hybrid welding of T-type structure of titanium sheet LI Chenbin, LIU Liming (Key Laboratory of Liaoning Advanced Welding and Joining Technology, Dalian University of Technology, Dalian 116024, China). pp 29 – 32

Abstract: Low powered laser-arc hybrid welding was used to weld T-type structure of titanium sheet. The welding joints were investigated via the optical microscopy, X-ray diffractometer. Results showed that laser could induce arc and enhance the penetrability of arc in laser-arc hybrid welding process and welding of T-type structure of titanium sheet was easily achieved. The close ripples form on the top surface of the welding seam, and the welding joint is full-penetration and gentile on the back. The welding seam is made up of α′-phase and β-phase. The acicular α′ is loose and disheveled because of the stirring effect of pulsed laser, pulsed TIG, spray of metal vapor and plasma. The contents of Al and Mn are maintained steadily, and there is no component segregation.

Key words: T-type structure; hybrid welding; titanium alloy

Control method for nugget size of resistance spot welding of three-layer steels with different thickness and strength SHEN Jie, LIN Haolei, ZHANG Yansong, CHEN Guanlong (Shanghai Key Laboratory of Digital Autobody Engineering, Shanghai Jiaotong University, Shanghai 200240, China). pp 33 – 36

Abstract: In order to study the nugget formation during resistance spot welding procers of three-layer steels with different strength and thickness, asymmetric electrodes were utilized to improve the nugget size and weldability. Finite element analysis was used to investigate the current density, temperature change and nugget sizes of the thinner side. Experiments were also carried out to analyze nuggets sizes at different welding time. The welding lobes under symmetric and asymmetric electrodes were established. The results showed that the current density and temperature field of the thinner side could be changed significantly as asymmetric electrodes were applied, which could facilitate the formation of nugget and widen the weldability of three-layer

sheets.

Key words: three layers; resistance spot welding; nugget size; welding lobe

Influence of heat sink on welding residual deformation and optimization analysis of parameters of heat sink ZHAO Lihua, ZHANG Kailin (Traction Power State Key Laboratory, Southwest Jiaotong University, Chengdu 610031 China). pp 37 -40

Abstract: The numerical simulations have been done for both the conventional metal active-gas welding (MAG) and the dynamically controlled low stress no-distortion (DC-LSND) MAG welding, and the measurement has been done for the DC-LSND experimental weldment as well, it is found that the simulating result is basically consistent with the measured data. Subsequently, the welding residual deformation of the partial side beam of bogie frame was selected as a research object, the optimization analysis of parameters of the heat sink had been done with the numerical simulation combining with optimization algorithm, and the alcording optimum scheme was obtained. The results showed that the control effect of welding residual deformation was obvious by the DC-LSND MAG welding with the optimum parameters.

Key words: dynamically controlled low stress no-distortion (DC-LSND) welding; heat sink; numerical simulation; optimization analysis; residual deformation

Toughness of welding heat affected zone in high strength steel with low welding crack susceptibility LAN Liangyun, QIU Chunlin, ZHAO Dewen, GAO Xiuhua (The State Key Laboratory of Rolling and Automation, Northeastern University, Shenyang 110819, China). pp 41 -44

Abstract: In this study, the submerged arc auto-welding technique was employed to weld the high strength steel with low welding crack suceptibility. The relationship between microstructural feature and toughness in different sub-zones of heat affected zone was analyzed in details. The results showed that the main microstructures in the coarse grained zone and fine grained zone are coarse bainite and fine quasi-polygonal ferrite, respectively. And corresponding average impact absorbed energy is 45 and 170 J, respectively. Electron back scattering diffraction (EBSD) analysis showed that the effective grain boundary of coarse bainite is prior austenite grain boundary and a number of sub-boundaries and dislocation exist inside the grain. The coarse effective grain size reduces the toughness of coarse grained zone. On the contrary, the average effective grain size of quasi-polygonal ferrite in the fine grained zone is about 5.3 μm. High angle grain boundary inhibits the propagation of crack and improves the toughness.

Key words: low welding crack susceptibility steel; toughness; heat affected zone; bainite

Effect of boron on microstructure and properties of high-boron iron-based alloy by plasma transferred arc LIU Zhengjun, LI Lechen, SU Yunhai, Zong Lin (School of Material Science and Engineering, Shenyang University of Technology, Shenyang 110178, China). pp 45 -48

Abstract: The iron-based composite materials of Fe-Cr-B-C hardfacing alloys were deposited on the surface of 20g steel by using plasma transferred arc (PTA). The effect of different B contents on microstructure and properties of surfacing layer was investigated by means of the X-ray diffraction (XRD), optical microscope (OM), scanning electron microscope (SEM), Rockwell hardness tester and wet sand abrasion tester. The result shows that the microstructure of the surfacing layer consists of supersaturated α-Fe dendrite solid solution, eutectic boride and carbides. The hard phases in the surfacing layer include Cr_2B, CrB_2, Fe_2B, Cr_7C_3 and B_4C etc. The amount of borides significantly increased with B content increasing, and the hardness and wear resistance of surfacing layer reached optimum value when B contents reached 5%. The hardness is 66.1 HRC and the weight reduction is 0.383 g. The wear resistance of surfacing layer decreased with the amount of boron further increasing.

Key words: plasma transferred arc; surfacing; boride; wear resistance

Prediction model of bead geometry shaped by rapid prototyping based on pulsed PAW XU Fujia[1], LÜ Yaohui[2], LIU Yuxin[2], XU Binshi[1,2], HE Peng[1] (1. Harbin Institute of Technology, State Key Laboratory of Advanced Welding and Joining, Harbin 150001, China; 2. Academy of Armored Forces Engineering, National Key Laboratory for Remanufacturing, Beijing 100072, China). pp 49 -52

Abstract: In this paper, rapid prototyping based on pulsed PAW technology is introduced. The Taguchi method is applied to design single bead forming experiments properly and then multi-group experimental data of weld width and height are obtained. The prediction model of bead geometry is developed by applying BP neural network based on genetic algorithm. It turns out that the model holds high prediction accuracy and generalization ability verified by error analysis and linear regression, which can predict single and multiple beads geometry accurately.

Key words: pulsed PAW; rapid prototyping; Taguchi method; genetic algorithm; BP neural network

Design of lower stress and flexible CCGA solder joints and reliability expectancy ZHAO Zhili[1,2], SUN Fenglian[1], WANG Lifeng[1], TIAN Chongjun[1] (1. School of Materials Science & Engineering, Harbin University of Science and Technology, Harbin 150040, China; 2. State Key Laboratory of Advanced Welding and Joining, Harbin Institute of Technology, Harbin 150001, China). pp 53 -56

Abstract: To improve the interconnect reliability of large-die area array package and reduce the stress concentration in solder joints under service load, the flexible interconnect structure for CCGA (ceramic column grid array) package and its solder joints shape are designed based on mechanics principle. Mechanical behaviors of the lower stress and flexible CCGA interconnect structure under shear load are studied by finite element method. Results showed that the designed copper tapered-funnel in both ends of copper column subjected to peak stress